ELSEVIER

Environmental Pollution 107 (2000) 1–20

ENVIRONMENTAL POLLUTION

www.elsevier.com/locate/envpol

Quantifying simultaneous fluxes of ozone, carbon dioxide and water vapor above a subalpine forest ecosystem

K.F. Zeller [a,*], N.T. Nikolov [b]

[a] *USDA Forest Service, Rocky Mountain Research Station, 240 W. Prospect, Ft. Collins, CO 80526, USA*
[b] *Oak Ridge National Laboratory, Environmental Science Division, PO Box 2008, Oak Ridge, TN 37831-6335, USA*

Received 15 March 1999; accepted 1 June 1999

Eddy covariance measurements from over a spruce-fir forest are presented and suggestions for improved methods are discussed.

Abstract

Assessing the long-term exchange of trace gases and energy between terrestrial ecosystems and the atmosphere is an important priority of the current climate change research. In this regard, it is particularly significant to provide valid data on simultaneous fluxes of carbon, water vapor and pollutants over representative ecosystems. Eddy covariance measurements and model analyses of such combined fluxes over a subalpine coniferous forest in southern Wyoming (USA) are presented. While the exchange of water vapor and ozone are successfully measured by the eddy covariance system, fluxes of carbon dioxide (CO_2) are uncertain. This is established by comparing measured fluxes with simulations produced by a detailed biophysical model (FORFLUX). The bias in CO_2 flux measurements is partially attributed to below-canopy advection caused by a complex terrain. We emphasize the difficulty of obtaining continuous long-term flux data in mountainous areas by direct measurements. Instrumental records are combined with simulation models as a feasible approach to assess seasonal and annual ecosystem exchange of carbon, water and ozone in alpine environments. The viability of this approach is demonstrated by: (1) showing the ability of the FORFLUX model to predict observed fluxes over a 9-day period in the summer of 1996; and (2) applying the model to estimate seasonal dynamics and annual totals of ozone deposition and carbon, and water vapor exchange at our study site. Estimated fluxes above this subalpine ecosystem in 1996 are: 195 g C m^{-2} $year^{-1}$ net ecosystem production, 277 g C m^{-2} $year^{-1}$ net primary production, 535 mm $year^{-1}$ total evapotranspiration, 174 mm $year^{-1}$ canopy transpiration, 2.9 g m^{-2} $year^{-1}$ total ozone deposition, and 1.72 g O_3 m^{-2} $year^{-1}$ plant ozone uptake via leaf stomata. Given the large portion of non-stomatal ozone uptake (i.e. 41% of the total annual flux) predicted for this site, we suggest that future research of pollution–vegetation interactions should relate plant response to actively assimilated ozone by foliage rather than to total deposition. In this regard, we propose the Physiological Ozone Uptake Per Unit of Leaf Area (POUPULA) as a practical index for quantifying vegetation vulnerability to ozone damage. We estimate POUPULA to be 0.614 g O_3 m^{-2} leaf area $year^{-1}$ at our subalpine site in 1996. Published by Elsevier Science Ltd.

Keywords: Ozone deposition; Plant ozone uptake; Carbon dioxide; Flux; Eddy covariance; Latent heat; Sensible heat; Ecosystem model; Ameriflux; Subalpine ecosystem

1. Introduction

Forest ecosystems are known to play an important role in carbon sequestration and the uptake and destruction of tropospheric ozone (O_3). Yet, this role and the budgets of tropospheric carbon dioxide (CO_2) and O_3 are uncertain in remote forested areas (Chameides and Lodge, 1992; Wofsy and Hollinger, 1998). With the broad governmental agency support of the new 'Ameriflux' program designed to continuously measure 'net CO_2 flux' and energy exchange in a variety of environments (Wofsy and Hollinger, 1998), it has become important to choose sites which represent key ecosystem types (such as subalpine areas) and provide valid data. Measurements of ecosystem fluxes at these sites will utilize the eddy covariance technique. Theoretically, this micrometeorological method is only feasible

* Corresponding author. Tel.: +1-970-498-1238; fax: +1-970-498-1010.

E-mail address: k.zeller@lamar.colostate.edu (K.F. Zeller).

0269-7491/99/$ - see front matter Published by Elsevier Science Ltd.
PII: S0269-7491(99)00156-6

over flat, uniform landscapes due to the stationarity and homogeneity assumptions necessary to simplify the turbulent continuity equation for mass. In practice, however, the eddy covariance technique has also been found to produce reliable results in rough terrain (Fitzjarrald and Moore, 1992) when vector rotation is applied (McMillen, 1988).

In 1987, the USDA Forest Service established the Glacier Lakes Ecosystem Experiment Site (GLEES) in southern Wyoming to conduct subalpine ecological research (Musselman, 1994). An Ameriflux installation is currently planned for this study location (Wofsy and Hollinger, 1998). Over the past 10 years, the Forest Service has collected a wealth of information on vegetation and the physical environment at GLEES including data on the ecosystem–atmosphere exchange of mass and energy. Zeller and Hehn (1995, 1996) successfully measured deposition of O_3 and energy fluxes at GLEES in the summer and winter of 1992 and in the winter of 1994. Data on fluxes of CO_2 were obtained at this site in August 1996.

The main objective of this paper is to provide a quantitative assessment of the 1996 seasonal dynamics and annual totals of key ecosystem fluxes at a subalpine site. We present eddy covariance measurements and model analyses of the concurrent CO_2, O_3, and water vapor fluxes over a high altitude forest at GLEES. We discuss problems related to interpretation of flux measurements in complex terrain using data from a 9-day period in the summer of 1996. Given measurement uncertainties, we explore the possibility of complementing instrumental data records with model simulations using FORFLUX (Nikolov, 1997) to better understand the long-term ecosystem–atmosphere exchange of mass and energy in a subalpine environment.

2. Experimental methods

2.1. Site description

GLEES is located at 3186 m elevation in the Snowy Range of the Medicine Bow National Forest in southern Wyoming, USA (41°22′N, 106°14.5′W). The research complex is described in detail by Musselman (1994). The study area is covered by an open forest dominated

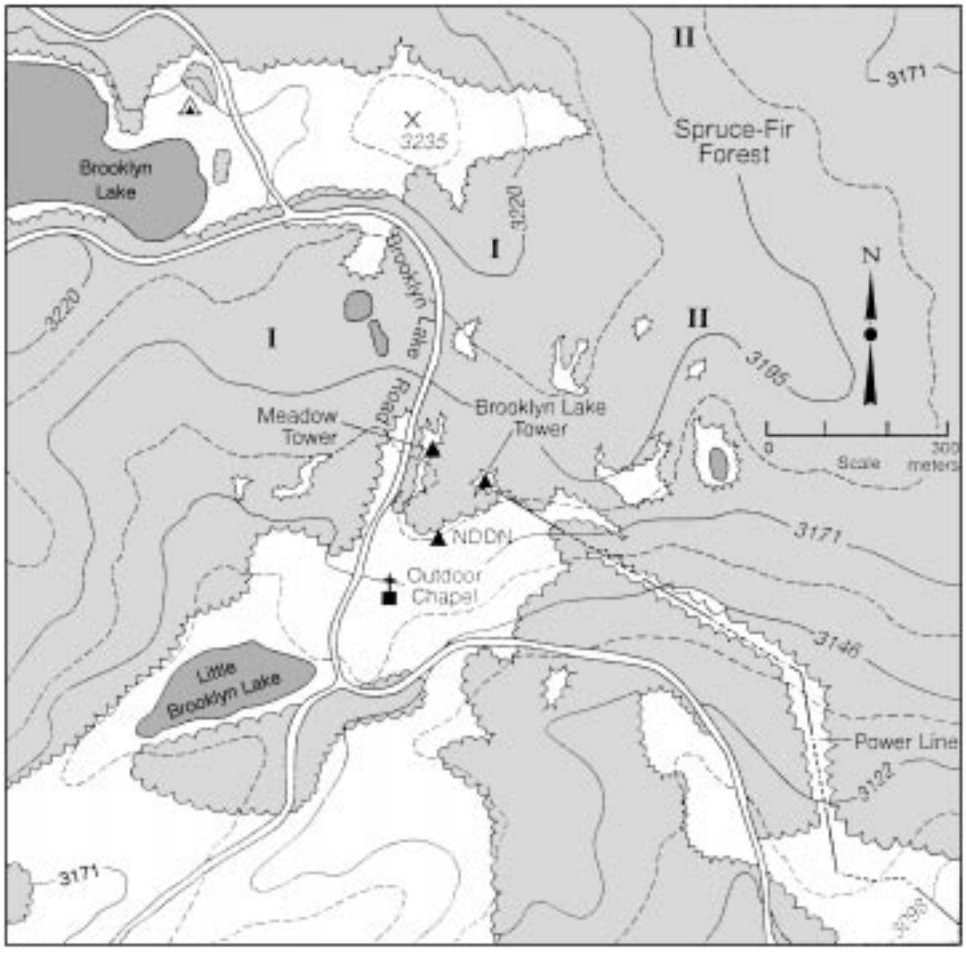

Fig. 1. Site map of Brooklyn Lake tower and surroundings.

by Engelmann spruce (*Picea engelmannii*) and subalpine fir (*Abies lasiocarpa*). The meteorological and flux data were collected from several heights on a 29-m tower (hereafter called the Brooklyn tower) situated in a 30-m wide forest opening (Fig. 1). Wind and CO_2 data were also collected from 1-m height at a 'wet' meadow site located 100 m west-northwest of the Brooklyn tower. This small tower is positioned at the east edge of a meadow and is separated from the Brooklyn tower by a uniform flat forested area. Measurements in the meadow are used to characterize the near-surface CO_2 concentration and wind field around the Brooklyn tower. The average height of the forest canopy at the Brooklyn tower is 17 m. For a neutrally stable atmosphere the calculated displacement height (d) is 11.7 m and the roughness length (z_o) is 1.7 m (Zeller and Hehn, 1996). For modeling purposes, we have estimated the leaf area index (LAI) of the surrounding forest to be 2.8 $m^2\ m^{-2}$.

Within 1 km of the tower, the terrain has a slope of +2.5% from west to east and −9.7% from north to south. In the direction of the predominant wind (i.e. west-northwest), the landscape is forested, and has a constant slope of 2.2% for about 1 km. The predominant wind direction above the canopy is 210° (south-southwest)–330° (northwest). Fig. 2 illustrates the effect of terrain on the half-hour wind vector ratio (w/u) at 23 and 1 m above the ground as a function of wind direction. It can be seen that at 23 m, the wind first flows uphill (positive w) from south-southwest through west-northwest, and then abruptly flows downhill as the wind direction swings farther from north. The topographic contour lines in Fig. 1 show a small ridge just east of the tower that causes the vertical flow change. The wind vector ratios measured at 1 m height on the meadow tower are predominantly negative. They are also plotted on Fig. 2 and discussed below.

This site is relatively complex from a standpoint of micrometeorological measurements. CO_2 has not been routinely measured at GLEES but O_3 concentrations have been documented by Wooldridge et al. (1997) and O_3 fluxes by Zeller and Hehn (1996).

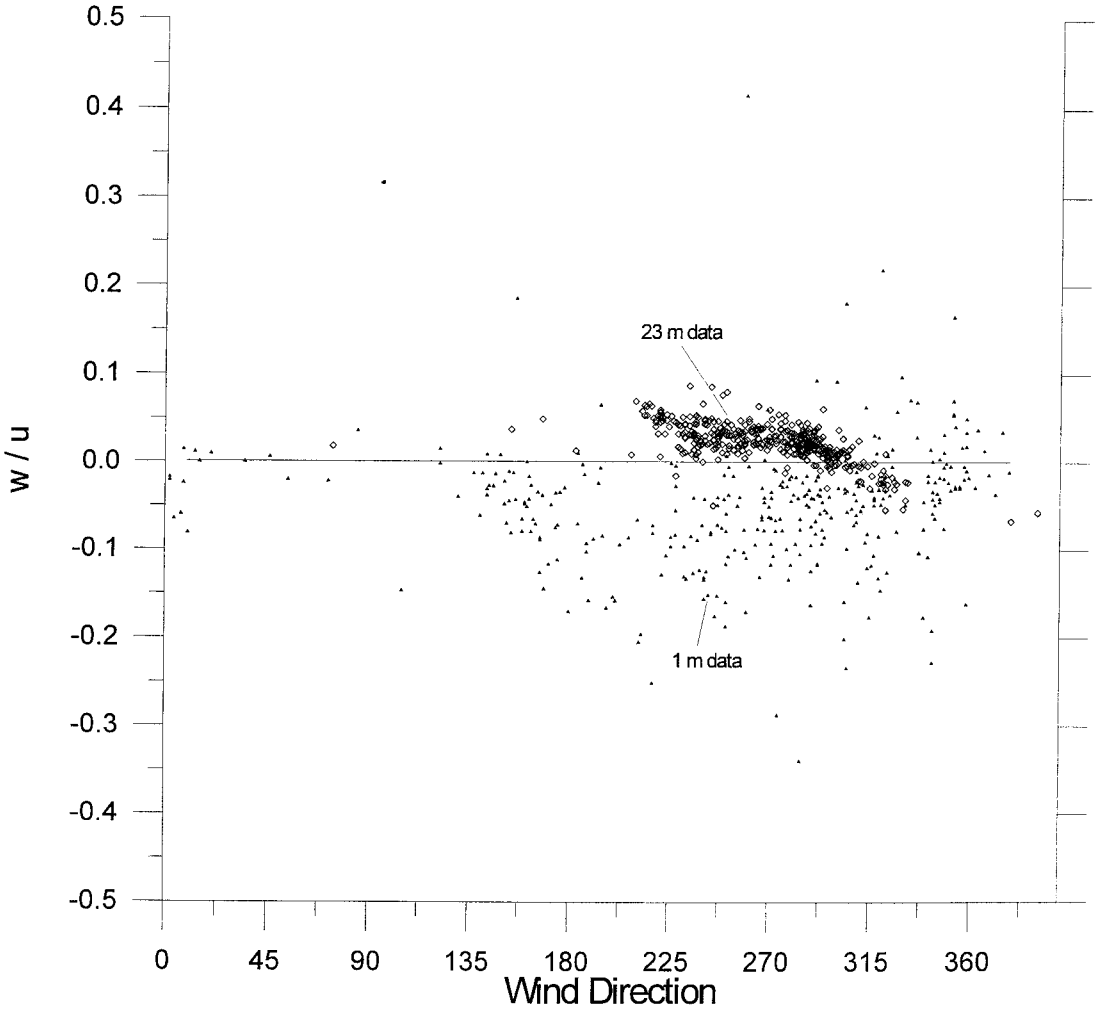

Fig. 2. Plot of half-hour wind vector magnitude ratio ($\overline{w}/\overline{u}$) as a function of wind direction for the period 30 July–8 August, 1996. Open diamonds (◇) are 23 m data and filled triangles (▲) are 1 m data. (A value of $w/u = 0.1$ is equivalent to 5.7° vertical angle.).

Table 1
List of eddy covariance instrumentation at Brooklyn Lake meadow site

Instrument or model	Height(s)	Type	Parameter	
TECO49 O_3 Analyzer	29	UV adsorption	c	O_3 concentration
Infrared gas analyzer	23	Open-path, infrared absorption	c, c'	CO_2 and H_2O concentration and fluctuation
	1		q, q'	
CAAM1 O_3 Analyzer	29	Chemiluminescence (fast response)	c'	O_3 fluctuation
RM Young Gill anemometer	23	Propeller	w, w′	Vertical wind
	29	Anemometer	u, u′	Horizontal wind
			v, v′	Horizontal wind
ATI, Inc. 15-cm anemometer	1	Sonic anemometer	w, w′	Vertical wind
			u, u′	Horizontal wind
			v, v′	Horizontal wind
Campbell Sc., Inc. krypton hygrometer	29	Light adsorption	q, q′	H_2O

2.2. Instrumentation and flux measurements

Micrometeorological and flux data were collected from 30 July to 8 August, 1996. This data represent 10 out of the 13 'core' measurement parameters and three out of the seven 'desired' parameters recommended by the Ameriflux science team (Table 2 in Wofsy and Hollinger, 1998).

The eddy covariance systems (Zeller et al., 1989; Massman et al., 1990) were deployed at 23 (6 m above canopy) and 29 m (12 m above canopy) on the Brooklyn tower. They measured fluxes of O_3, CO_2, momentum, sensible and latent heat as well as concentrations of O_3 and CO_2, temperature, wind speed and wind direction. Standard meteorological sensors were permanently mounted at 10 and 29 m for routine weather measurements (Musselman, 1994). O_3 flux was measured at 29 m employing a Gill[1] UVW anemometer and a Chemiluminesence Ambient Air Monitor (CAAM1) (Ray et al., 1986). CAAM1 was continuously calibrated using a TECO49 commercial UV adsorption instrument. For O_3 measurements, ambient air was sampled from 29 m height through a 31-m long (1.6-cm inside diameter) Teflon tube. The lag time of the intake system (t_l) was typically 2.4 s. A second TECO49 instrument was operated at 3 m height near the base of the tower to measure below-canopy O_3 concentration. Fluxes of CO_2 and water vapor were measured at 23 m on the Brooklyn tower using an open-path, infrared absorption gas analyzer (Auble and Meyers, 1992). CO_2 measurements were also made at 1 m height on the meadow tower using a second open-path CO_2 analyzer. The slow responding CO_2–H_2O analyzer (LICOR 6262), used for continuous calibration of the CO_2 instrument deployed at 23 m, malfunctioned just prior to the 9-day period presented here. The Gill UVW anemometers have been used on the Brooklyn tower instead of sonic anemometers for their greater durability in a harsh alpine environment and were used in this study because two sonics were not available. The measurements taken at the meadow at 1 m height employed a 15-cm sonic anemometer, and a second open-path, infrared absorption CO_2 gas analyzer. Table 1 summarizes the flux instrumentation used in this study.

The 15-Hz eddy deviations of O_3 and CO_2 concentrations, $c' = c - \overline{c}$ (where $\overline{c}$ is a 200 s recursive filter average concentration) were multiplied by the turbulent wind components u', v' and w', and then averaged over a halfhour sampling period (McMillen, 1988) to obtain the vertical flux (F_c) (μg m^{-2} s^{-1}) after a vector coordinate rotation for the $\overline{w} = 0$ streamline, i.e.:

$$F_c = \overline{w'(t)c'(t - t_l)} \quad (1)$$

Here, negative F_c indicates downward flux. Fluxes of momentum, sensible and latent heat were obtained likewise. The coordinate rotation does not affect the scalar flux sign and only slightly influences measured flux magnitudes. Fluxes with associated streamlines within $\pm 3°$ (at 23 m) and $\pm 8°$ (at 29 m) of the horizontal account for 98% of the data presented here (note that $w/u = 0.1$ is equivalent to 5.7° in Fig. 2). Gill UVW anemometer data were corrected in real time for the inherent cosine response (Massman and Zeller, 1988).

Businger's list of measurement concerns (Businger, 1986) was adopted for evaluation and editing of the eddy covariance data. The O_3 flux corrections for sensible and latent heat effects implemented Eq. (12) by Leuning and Moncrieff (1990). The corrections of CO_2 flux for an open-path system were made using Eq. (5) by Leuning and Moncrieff (1990). Hereafter, we refer to

[1] The use of trade and company names is for the benefit of reader; such use does not constitute an official endorsememt or approval of any service or product by the USDA to the exclusion of others that may be suitable.

the latter correction as LM. We discuss the effect of these corrections below in addition to an empirical 'advection' correction based on Lee (1998) and Baldocchi (personal communication). The latent heat flux obtained with a krypton hygrometer at 29 m height was corrected for the oxygen influence (Tanner and Greene, 1989). Data below the scale height of 23 m (i.e. $h_t < |\overline{w'c'}/(\overline{\partial c}/\partial t)|$) for CO_2 and below 29 m for O_3 were culled. A digital butterworth filter was applied in real time to account for aliasing. Corrections for instrument design and separation can theoretically increase flux magnitudes by 20–80% in uniform flat terrain (Zeller et al., 1989; Massman et al., 1990) when using a Gill anemometer with faster responding instruments (e.g. the CO_2 and H_2O sensors). These corrections tend to increase the random noise in reported fluxes, but do not affect flux direction and are much less important in the above-canopy roughness layer where transporting eddies are relatively large. Hence, the flux data presented here were not corrected for such effects.

Neutral stability statistics (Panofsky and Dutton, 1984; Schuttleworth, 1989) during this study for wind, temperature, CO_2 and O_3 are fairly consistent and are equivalent to results from other field studies. For example, σ_w/u^* was consistently 1.2 ± 0.1 at 29 m and 0.95 ± 0.1 at 23 m compared to 1.3 for flat terrain. Dimensionless wind shear, $\phi_m = \overline{kz/u^*}(\overline{\partial u}/\partial z)$, was consistently 1.3 ± 0.3 at 29 m and 1.1 ± 0.3 at 23 m where $u_* = \sqrt{-\overline{w'u'}}$ was calculated from the momentum flux.

2.3. Overview of the FORFLUX model

Nikolov (1997) developed a biophysical model (FORFLUX) to study the seasonal exchange of CO_2, O_3, and energy between terrestrial ecosystems and the atmosphere. The model mechanistically couples major ecosystem processes controlling the flows of carbon and water implementing recent concepts in plant eco-physiology and soil hydrology. FORFLUX consists of four interconnected modules: a leaf photosynthesis model, a canopy flux model, a soil heat-, water- and CO_2-transport model, and a snow pack model.

Leaf-level net photosynthesis and water-vapor flux are computed by the LEAFC3 submodel (Nikolov et al., 1995). This submodel simulates coupled interactions between mesophyle biochemical reactions, stomatal conductance and the leaf energy balance. LEAFC3 predicts four state variables, which are used as input to the FORFLUX canopy module, i.e. net photosynthesis rate, stomatal conductance to water vapor, leaf temperature and leaf boundary-layer conductance. These variables are obtained from the solution to a system of seven simultaneous equations.

The FORFLUX canopy module scales LEAFC3 output to a canopy level. This is achieved by numerical integration of the LEAFC3 model over the canopy LAI. The integration takes into account: (1) the short- and long-wave radiative transfer inside the canopy; (2) variation of foliage photosynthetic capacity with canopy depth; (3) wind speed attenuation throughout the canopy; and (4) rainfall interception by foliage elements. The canopy submodel also calculates above-ground woody respiration and seasonal phenological changes in stand LAI. The radiative transfer module implements a four-stream analytical solution to the multiple scattering equation and is based on work by Ross (1981), Sellers (1985) and Camillo (1987). The algorithm accounts for spectral changes of the incident solar flux inside the canopy caused by the selective radiation absorption of green leaves. The model uses leaf clumping and angular distribution of foliage elements to estimate penetration and absorption of the direct and diffuse radiation in the visible (380–700 nm), near-infrared (700–1500 nm) and thermal (>1500 nm) bands. Leaf photosynthetic capacity is assumed to decline with canopy depth according to data and models by Hirose and Werger (1987) and Hirose et al. (1988). The attenuation of horizontal wind speed inside the canopy is simulated using the phenomenological model of Albini (1981) as modified by Massman (1987). In FORFLUX, wind speed controls the energy balance of leaves by modifying the leaf-boundary layer conductance and air humidity at the leaf surface. Rainfall interception is computed as a function of canopy water storage capacity, rainfall intensity and current evaporative demand employing an analytical interception model by Massman (1983). Net photosynthesis of wet foliage is estimated by the LEAFC3 model assuming that evaporation completely suppresses transpiration, and wetness does not adversely affect CO_2 assimilation capacity of leaves.

The soil module simulates the dynamics of moisture and temperature within the soil profile, soil-surface evaporation and CO_2 efflux from soil due to root and microbial respiration. Vertical transport of water and heat in soil is modeled using principles of diffusion theory (Hillel, 1982; Campbell, 1985; Feddes et al., 1988). The effect of soil heterogeneity on field-scale fluxes is simulated employing the Bresler–Dagan concept (Bresler and Dagan, 1983; Dagan and Bresler, 1983; Dagan, 1993). The latter can be summarized as follows. A spatially variable field is approximated by an array of non-interacting homogeneous soil columns, each one of which is characterized by a unique set of hydraulic parameter values. These values are estimated from observed probability distributions of soil properties across the horizontal plane. The hypothesis is that one can obtain an accurate estimate of the mean scalar fluxes at the field scale by computing scalar transports in numerous columns (using a 1-dimensional model) and then averaging the output horizontally. The theoretical justification behind such an approach is that although soil

properties vary in a 3-dimensional space, the length scale of variation is much larger in the horizontal domain than it is in the vertical one. Thus, vertical soil variability would only have a small effect on the average field flow. Soil surface evaporation is computed from an explicit analytical solution of the surface energy balance equation, which accounts for atmospheric stability effects in the surface boundary layer. The CO_2 efflux from soil is estimated using a bulk-parameterization approach, which considers the effect of soil moisture, temperature and clay content on CO_2 production. The temperature factor is computed using the exponential function of Kirschbaum (1995) and soil respiration data summarized by Peterjohn et al. (1994). The effect of volumetric moisture on soil CO_2 release is described using experimental data and models by Schlentner and Van Cleve (1984) and Grant and Rochette (1994).

The snowpack module accounts for the dynamics of snow accumulation and melt on the ground. Incoming precipitation is partitioned into snow- and rainfall based on ambient temperature (Wigmosta et al., 1994). The model does not consider snow interception by the canopy and, hence, all snowfall is added to the ground storage. Snowpack is depleted through sublimation and melting. Both processes are assumed to occur at the snow–atmosphere interface and to be a function of the snowpack energy balance (Male and Gray, 1981). Radiation absorption by the snowpack is computed from incident visible, near-infrared and thermal irradiances and corresponding snow reflectances. Snow albedos in the visible and near-infrared wavelength are estimated using the physical model of Marshall (1989), which accounts for effects of snow grain radius, impurity content, snow depth, solar zenith angle and cloud cover. Snow depth and soot concentration primarily influence visible albedo while grain size and zenith angle mainly affect near-infrared snow reflectance.

All biophysical interactions in the FORFLUX model are computed hourly while model projections are produce on hourly or daily time step. FORFLUX requires for input hourly values of ambient temperature, relative humidity, incident short-wave radiation, precipitation and above-canopy wind speed. Species physiology is characterized in the model by 20 parameters. Tables A1 and A2 in the Appendix list the species and site-specific input parameters and their values used in this study. Model output includes temporal courses of net ecosystem carbon and water fluxes and their components, such as vegetation net primary production (NPP), canopy photosynthesis and stomatal conductance, woody respiration, soil CO_2 efflux, canopy transpiration and rainfall interception, soil evaporation, snow melt and sublimation, surface runoff and subsoil drainage.

Compared to other biophysical models such as BIOMASS (McMurtie et al., 1990, 1992), FOREST-BGC (Runnung and Coughlan, 1988; Running and Gower, 1991), PnET (Aber and Federer, 1992), and TCX (Bonnan, 1991a,b), the FORFLUX model is notable for the following innovations:

1. Canopy fluxes are estimated by a vertical integration of the LEAFC3 model (Nikolov et al., 1995) which mechanistically couples photosynthesis, stomatal conductance and energy balance at the leaf level. This provides a more accurate simulation of the gas and energy exchange at the canopy level compared to other models, which do not incorporate feedbacks between latent heat flux and CO_2 uptake.
2. The transport of water and heat in soil is modeled employing physical principles of diffusion theory (Feddes et al., 1988) and explicitly accounting for effects of soil heterogeneity on field-scale fluxes (Dagan, 1993). This approach is expected to yield predictions of soil moisture dynamics, which are far more robust than those provided by various soil-bucket approximations used in other ecosystem models. To our knowledge, FORFLUX is the only biophysical model which combines a detailed formulation of canopy processes with a physically based stochastic algorithm for simulating heat and water flow in soil.
3. Root–shoot communication is modeled using a new scheme, which incorporates the joined effect of root chemical and hydraulic signaling on leaf stomatal conductance (Tardieu and Davies, 1993). This allows for a realistic simulation of the observed feedback between transpiration rate and stomatal sensitivity to adverse soil conditions such as drought and freezing.

2.3.1. Simulation of O_3 deposition

The FORFLUX model predicts total O_3 deposition (F_{O_3}) as a sum of three fluxes, i.e. plant O_3 uptake via leaf stomata, O_3 deposition to non-transpiring plant surfaces, and O_3 flux absorbed by the ground (i.e. soil or snow surface), i.e.:

$$F_{O_3} = \frac{\Delta C_{O_3}}{r_a + 1/g_{cs}} + \frac{\Delta C_{O_3}}{r_a + 1/g_{ct}} + \frac{\Delta C_{O_3}}{r_a + r_u + r_{bs} + r_{is}}. \quad (2)$$

In this equation, ΔC_{O_3} is the O_3 concentration gradient (ppbv) between the active surface and a reference height above the canopy (assuming a zero O_3 concentration at the surface; ΔC_{O_3} equals the measured ambient O_3 concentration with a negative sign); g_{cs} is the foliage canopy conductance to O_3 (m s^{-1}) (i.e. the sum in parallel of stomatal and leaf boundary-layer conductances); g_{ct} is the plant surfacial (or cuticular) conductance to O_3 deposition (ms^{-1}); r_a and r_u are the

above- and within-canopy aerodynamic resistances, respectively; r_{bs} is the soil boundary-layer resistance; and r_{is} is the soil intrinsic resistance (all resistances have units of s m^{-1}). The canopy O_3 conductance (g_{cs}) is the most important one of all conductances and resistances within the soil–plant–atmosphere continuum. It is estimated by integrating individual leaf O_3 conductances (g_{lt}) over the canopy LAI (L_t m^2 m^{-2}), i.e.:

$$g_{cs} = \int_0^t g_{lt} dL, \tag{3}$$

where g_{lt} is calculated from the leaf stomatal (g_{sv}) and boundary-layer (g_{bv}) conductance to water-vapor exchange using the formula:

$$g_{lt} = \frac{g_{sv} g_{bv}}{1.315 g_{sv} + 1.508 g_{bv}}. \tag{4}$$

In Eq. (4), 1.508 and 1.315 are ratios of water vapor and O_3 diffusivities in still air and in the leaf-boundary layer, respectively. These are calculated from data presented in Table 2 by Massman (1998). Vapor conductances, on the other hand, are predicted by the coupled leaf photosynthesis–transpiration module (LEAFC3) of the FORFLUX model.

Canopy aerodynamic resistance (r_a) is estimated using an empirical equation derived from the measured momentum flux at GLEES:

$$r_a = \frac{19}{U^{1.35}}, \tag{5}$$

where U is the measured horizontal wind speed (m s^{-1}) above the canopy. The plant surfacial conductance is estimated as $g_{ct} = 1.4 \times 10^{-5}$ m s^{-1} based on data by Kerstiens and Lendzian (1989) and Massman and Grantz (1995). The within-canopy aerodynamic resistance is assumed to be eight times greater than r_a, i.e.:

$$r_a = 8 r_a. \tag{6}$$

The surface boundary-layer resistance to O_3 is computed from the ground boundary-layer conductance to water vapor ($g_{bs,v}$ m s^{-1}) using the formula:

$$r_{bs} = \frac{1.37}{g_{bs,v}}, \tag{7}$$

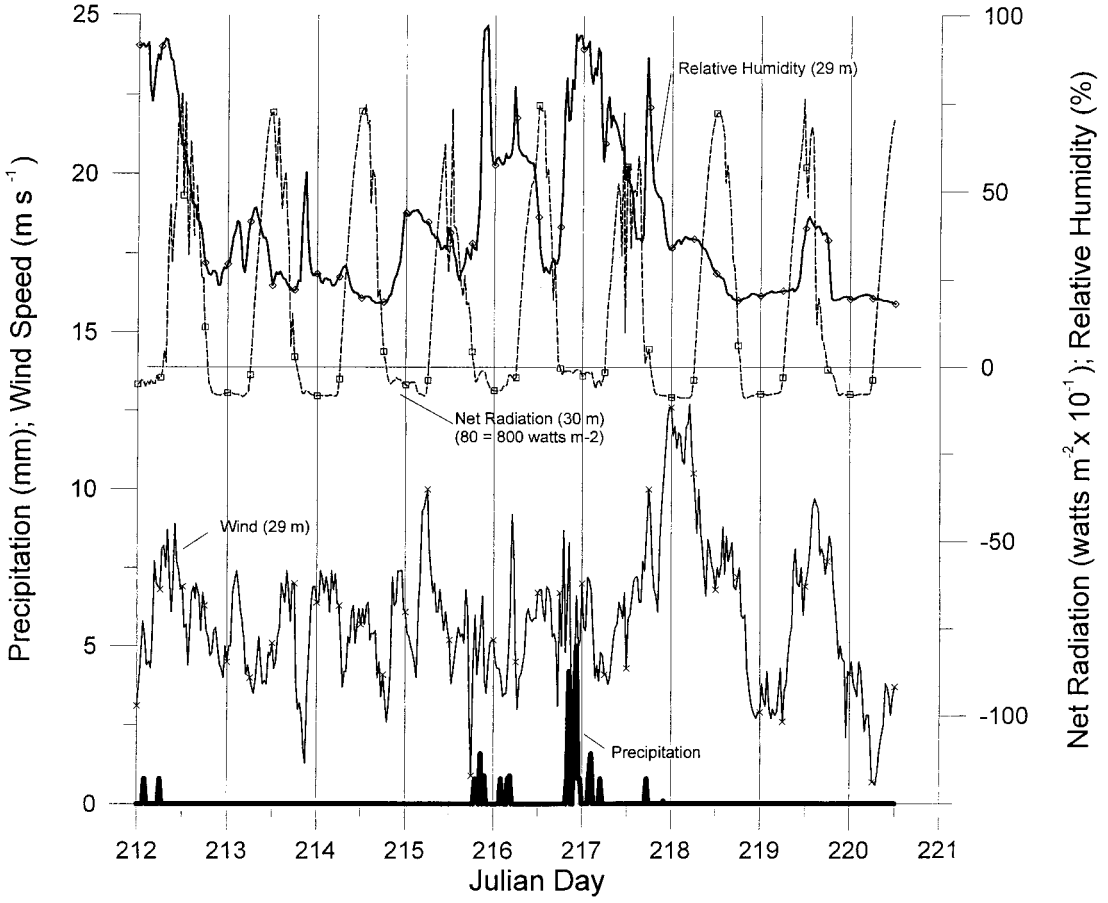

Fig. 3. Upper: half-hour average relative humidity (solid line, open diamonds); half-hour net radiation (dashed line, open squares). Lower: half-hour wind speed at 29 m (solid line, ex's); precipitation (thick solid line) for the period 30 July–8 August, 1996.

where $g_{bs,v}$ is produced by the ground evaporation module of the FORFLUX model. This module solves exactly the surface energy balance equation while accounting for atmospheric stability effects on the boundary-layer conductance. The constant 1.37 is a ratio of molecular diffusivities of O_3 and water vapor assumed in the surface boundary layer.

The intrinsic soil resistance is considered to be constant in time. Based on information on soil resistances to O_3 deposition gathered by Turner et al. (1974) and van Pul (1992), it was assumed $r_{is} = 410$ s m^{-1} for bare soil. In the presence of a snow pack, r_{is} is set to 6000 s m^{-1} as suggested by measurements of Zeller and Hehn (1995).

3. Results and discussion

3.1. Surface Meteorology

Fig. 3 depicts the 9-day time series of measured half-hour values of net radiation, relative humidity, wind speed and precipitation. Air temperature is graphed on the bottom of Fig. 4. Four short precipitation events occurred around midnight on Julian days 212, 216, 217 and 218. Rainfall interrupts the fast response open-path sensors. Therefore, CO_2 fluxes during these periods are automatically eliminated. The use of Gill anemometers and the air intake system for O_3 allows continuous sampling of O_3 fluxes during light rainfall. We assume that light rainfall in the turbulent canopy boundary layer has a negligible effect on measured fluxes and, thus, do not correct for it. Since sensible and latent heat fluxes are intermittently affected by precipitation, hours having abnormally high or low variances are also routinely culled (i.e. sensible: $>1.2°C^2$ and $<0.0001°C^2$; latent: >0.4 g^2 m^{-6} and <0.0001 g^2 m^{-6}).

3.2. O_3 and CO_2 concentrations

Temporal variations of O_3 and CO_2 concentrations are presented in Fig. 4. There is some diurnal correlation between temperature and O_3 concentration

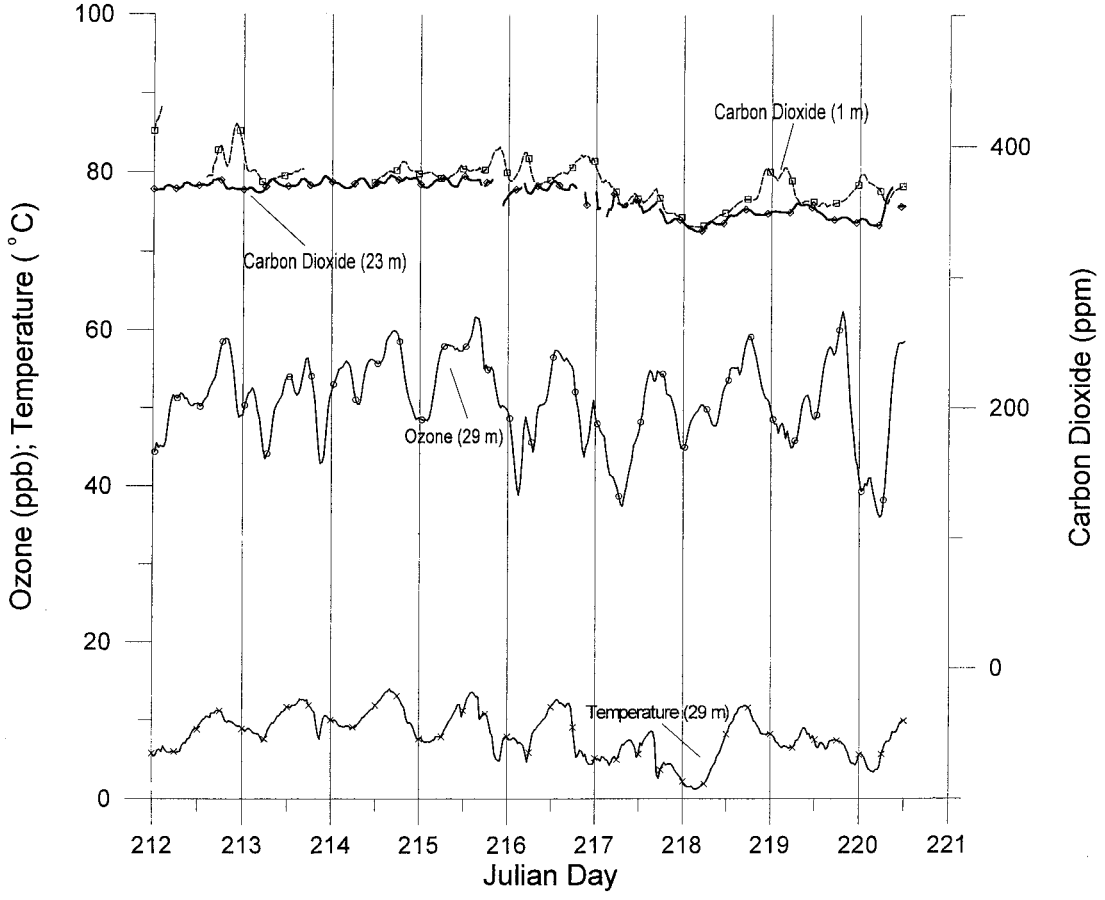

Fig. 4. Half-hour average CO_2 concentration (23 m solid line, open diamonds; 1 m O_3 concentration (dashed), O_3 concentration (solid line, open circle) and temperature (solid line ex's) for the period 30 July–8 August, 1996.

typically observed with O_3 monitoring. CO_2 concentrations are less accurate as they are obtained by highly sensitive fast-response sensors. However, the measured values average 377 ppm over the 9-day period. Half-hour variations of concentration at 1 and 23 m height are noisier than typically measured with slower-response instruments.

3.3. Measured vertical gradients

The measured vertical gradients of O_3, CO_2 and temperature are portrayed in Fig. 5. Positive values indicate increase of concentration with height. Thus, a positive gradient is associated with a negative (downward) flux, and a negative gradient implies a positive (upward) flux. In accordance with expectations, temperature gradients are greater near the surface as seen from the comparison of records from 10 and 3 m, and between 29 and 10 m height. The effect of enhanced night-time turbulent mixing on gradients of temperature and O_3 concentrations can be seen on days 215 and 218 when high wind speeds at night cause measured gradients to approach zero. To some extent this is also true for CO_2 concentrations. The CO_2 gradient is calculated from the open-path sensors, which are separated vertically by 22 m and horizontally by 100 m.

3.4. Energy fluxes and energy balance

The diurnal dynamics of momentum, sensible and latent heat fluxes are presented in Fig. 6 along with the soil heat flux. The 24-h average residuals of the daily energy balance ($R_n - G - H - \mathrm{LE}$) ending at midnight on each day are plotted on Fig. 6. These values are positive through JD 215, missing JD 215 through 217 due to night-time precipitation, and are positive but lower in value after JD 218. Daily residuals closely follow the temperature record for the sampling period (Fig. 4). This might indicate that the ecosystem is storing and releasing energy on a scale of several days. The effect of a possible energy storage and advection (Lee, 1998) can also be seen on the energy balance plot for the 9-day period (Fig. 7). Note that the TERM (R_n–G) is larger (positive values) than ($H + \mathrm{LE}$) during daytime and smaller (negative values) at night.

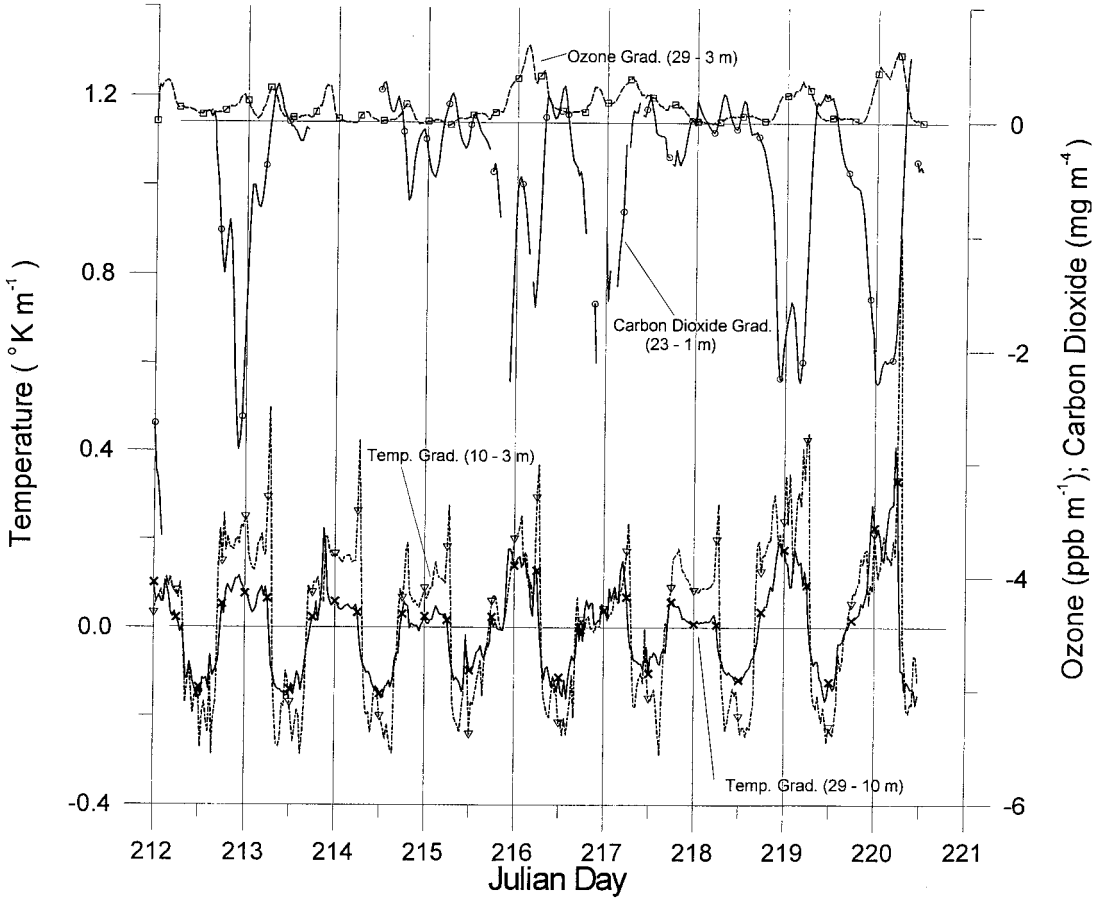

Fig. 5. Half-hour average 29–3 m O_3 gradient; 23 –1 m CO_2 gradient; and 29–10 m, and 10–3 m temperature gradients for the period 30 July–8 August, 1996.

3.5. O_3 and CO_2 fluxes

The eddy covariance measurements shown in Fig. 8 are consistent with respective vertical gradients (Fig. 5). The local time rate of CO_2 concentration change, $\int_0^h \frac{\partial \overline{c}}{\partial t}\delta z$, in the canopy layer was estimated from measured data as $((\Delta\overline{c}/\Delta t)_{h2} - (\Delta\overline{c}/\Delta t_{h1})\Delta z$, where $h=1$ and 23 m for CO_2, and 3 and 29 m for O_3. This estimate, also considered a storage term (Lee, 1998), is plotted for CO_2 and O_3 in Fig. 8. When this value was significant compared to measured O_3 eddy flux (e.g. $>20\%$), the stationarity assumption in Eq. (1) was judged to be violated and the associated eddy flux term was culled. However, for the CO_2 flux analysis discussed below, we kept track of this storage term and did not cull the corresponding CO_2 flux unless it was greater than 100%. Unfortunately, the corrected CO_2 flux (in Fig. 8) is not continuous due to either lack of information to complete the corrections or due to the presence of interfering atmospheric conditions. Such data losses are inevitable when using the eddy covariance technique and give an idea of the data gaps one can expect from CO_2 flux measurements in rough terrain.

3.5.1. Carbon dioxide fluxes

The CO_2 fluxes are presented in Fig. 8 as three superimposed data records. The three records illustrate the analyses problems associated with using the eddy covariance technique to measure CO_2 exchange in complex terrain. The thin line represents the calibrated 'raw' flux as measured prior to corrections. The darker dashed line (only discernible during night-time hours) shows the result of applying the LM correction for open-path sensors. This correction is very large. It varies from $+0.5\pm0.1$ mg m^{-2} s^{-1} during daytime to -0.15 ± 0.05 mg m^{-2} s^{-1} at night for the sensible heat term, and from $+0.08\pm0.03$ mg m^{-2} s^{-1} (daytime) to -0.002 ± 0.002 mg m^{-2} s^{-1} (night-time) for the latent heat term. The sensible heat term in the LM correction accounts for 85% of the adjustment and the latent heat term for the remaining 15%. The CO_2 flux resulting from the LM correction is near zero for most nights and near zero and random during daylight for days 215–219. For the CO_2 fluxes measured by eddy covariance in complex terrain, Lee (1998) suggests an advection correction of the form $\overline{w}_r(\overline{c}_r - <c>)$ and a storage correction to account for the night-time loss of CO_2 below the flux

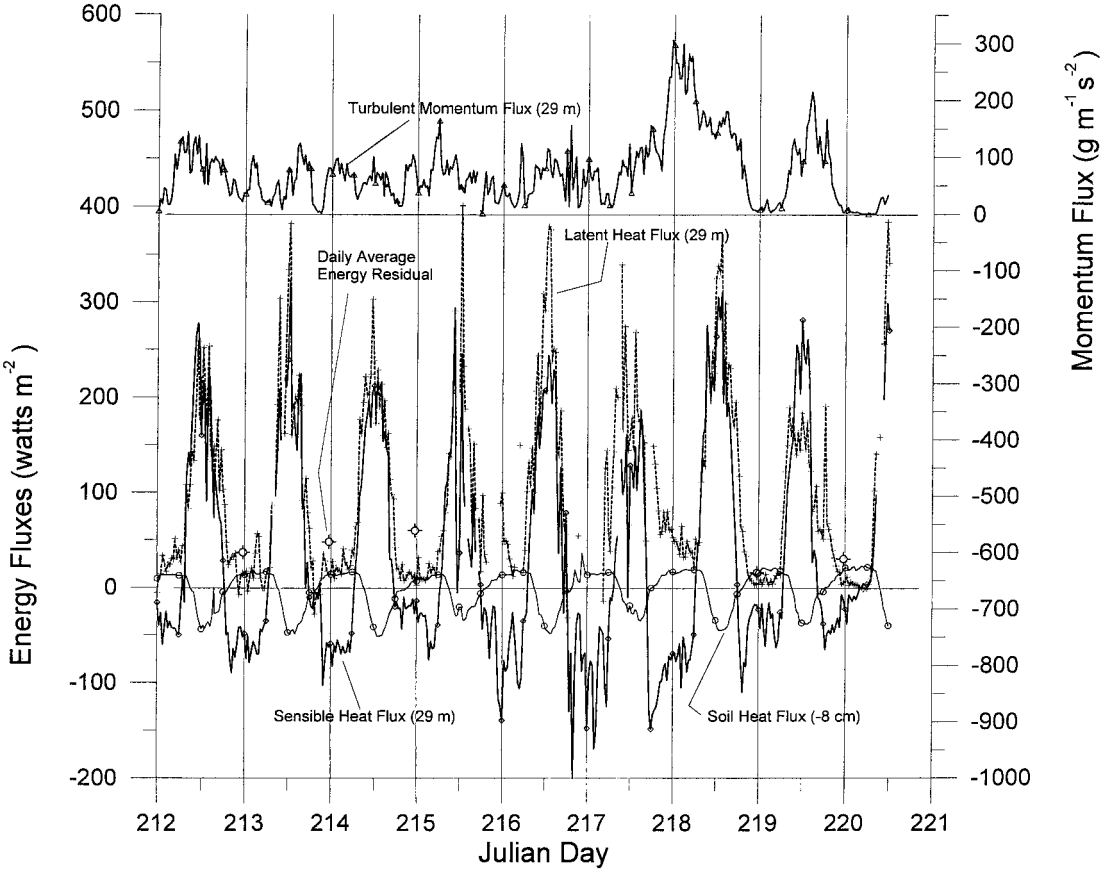

Fig. 6. Half-hour average 29 m turbulent momentum flux (Reynold's sress) (solid line, open triangle); 29 m sensible heat energy flux (solid line, open diamond); 29 m latent heat energy flux (dashed line, plus sign); −8 cm soil heat flux (thin solid line, open circle); and 24 h energy balance average (plus sign superimposed with open circle) for the period 30 July–8 August, 1996.

sampling height. Baldocchi (personal communication) suggests the correction $\overline{w_a(\overline{c}_r - < c >)}$. Here w_a is the difference between the measured vertical velocity, w_r, and a mean vertical velocity (w_θ) which depends on terrain and wind direction (i.e. $w_a = w_r - w_\theta$); c_r is the scalar concentration at reference height; and $< c >$ is the mean scalar concentration in the layer below the sampling height. Based on the observed large CO_2 gradients (Fig. 5), and the small magnitude of the corrected night-time flux, we conclude that the true CO_2 flux is not seen at 23 m and that an advection phenomena is occurring at our Brooklyn site. Due to the random fluctuation of the CO_2 storage term, the latter was not included in the correction as suggested by Lee (1998).

We attempted an advection correction (Lee, 1998; Baldocchi, personal communication). To this end, we used data on vertical wind velocity (w_r) measured at 23 m (Fig. 2) to compute a wind direction–terrain dependent vertical velocity (w_θ) to obtain w_a. Even though the term $(c_r - < c >)$ is consistently negative at night and positive during daylight, w_a at 23 m fluctuated widely making the correction $\overline{w_a(\overline{c}_r - < c >)}$ vary randomly between ± 0.2 mg m^{-2} s^{-1}. We also tried to use vertical wind velocity recorded at 1 m at the meadow site to estimate w_a but obtained a similarly unsatisfactory fluctuating result. Nevertheless, we judge that for our site, the wind data measured at 1 m better represent the near surface advection of air and CO_2 compared to those obtained at 23 m. Baldocchi (personal communication) suggested that w_θ and $\overline{w_a(\overline{c}_r - < c >)}$ should be established as averages using a long time series and that the correction is best applied as a diurnal function. Without the benefit of a complete CO_2 profile, but based on the CO_2 gradient in Fig. 5 and the slower wind speed measurements at 1m, we hypothesize that CO_2 is most likely being confined to the lower 1–2 m atmospheric layer. We also chose to use the friction velocity (u^*) at 1 m as a parameter to advect CO_2 in the surface layer since it is an indication of both air movement and turbulence. Hence, we employed $\overline{-u_*(\overline{c}_r - < c >)}$ as an empirical estimate for the advection. The result from this correction plus the LM correction is shown as a heavy solid line in

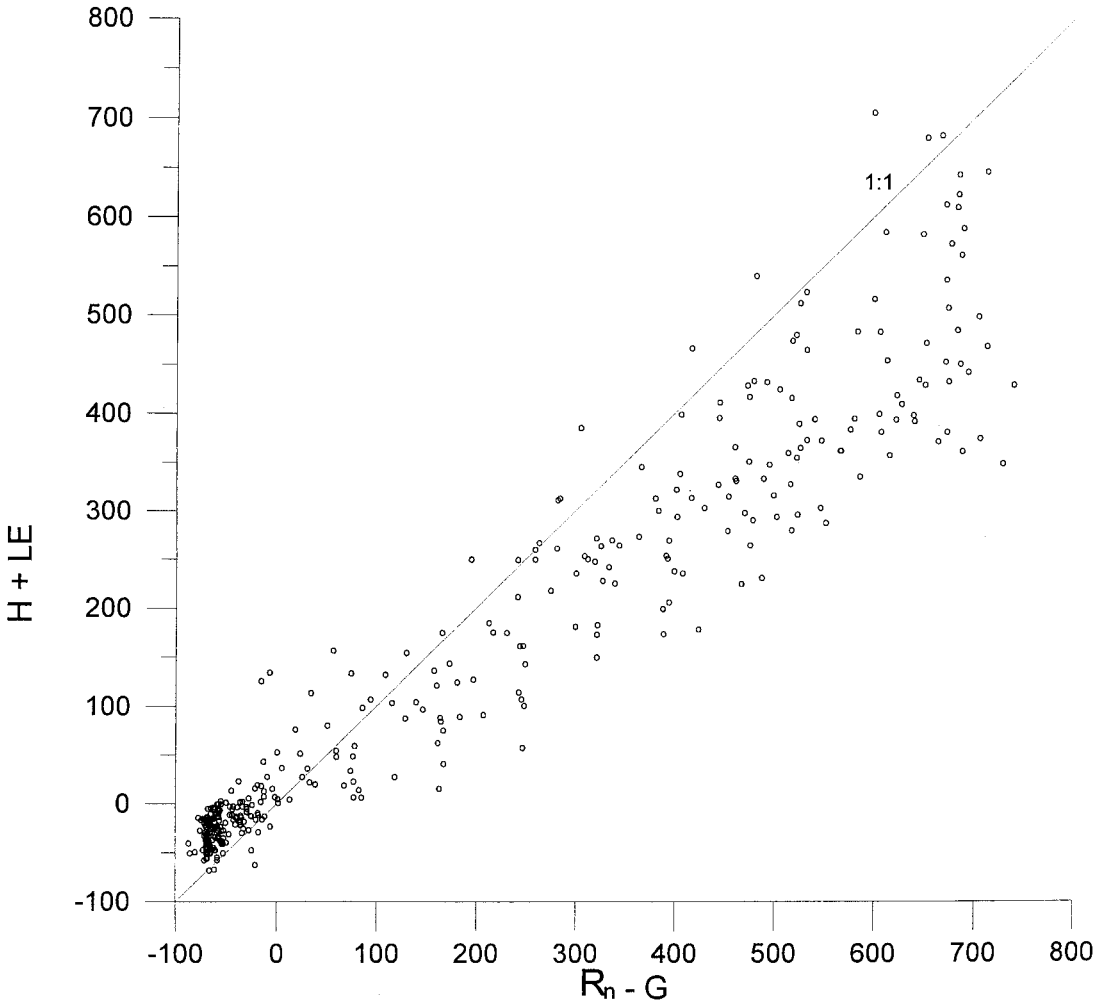

Fig. 7. Half-hour energy balance plot of H + LE verses $R_n - G$ (open circles) for the period 30 July–8 August, 1996.

Fig. 8. This approach yielded an average nighttime (17:30–05:30) convection correction value of +0.08 mg $m^{-2}s^{-1}$ and an average daytime (07:30 am to 13:00 pm) convection correction of −0.03 mg m^{-2} s^{-1} with a linear transition between the two values occurring from 05:30 to 07:30 MST and from 13:00 to 17:30 MST.

The corrected CO_2 flux varies from −1.0 mg m^{-2} s^{-1} to near zero during daytime and averages about $+0.25 \pm 0.2$ mg m^{-2} s^{-1} at night. Note that daytime corrections are small. Thus, the solid line in Fig. 8 representing fully corrected CO_2 flux is almost congruent with the dashed line of the LM correction during daytime. These flux results are similar to summertime CO_2 exchange rates measured over a deciduous forest near Oak Ridge, TN (35°N, 84°E) by Greco and Baldocchi (1996) who report daytime maximum of −1.1 mg m^{-2} s^{-1}, and night-time average of +0.18 mg m^{-2} s^{-1}. However, they are lower than daytime maxima of −0.35 mg m^{-2} s^{-1}, and night-time mean of +0.22 mg m^{-2} s^{-1} observed over a boreal black spruce forest in Saskatchewan, Canada (54°N, 105°W) by Jarvis et al. (1997).

3.5.2. O_3 fluxes

The O_3 flux record is presented at the bottom of Fig. 8 along with the O_3 storage parameter. O_3 deposition is shown as a downward flux. Corrections of the O_3 flux for a closed-path system were small, i.e. ±0.015 (μg m^{-2} s^{-1}. Maximum O_3 uptake occurs midday and ranges from −0.5 to −0.6 μg m^{-2} s^{-1}. Deposition rates are relatively high during night-time hours of JD 215 and 216 when atmospheric mixing was weak but O_3 concentration declined by more than 20 ppb, and again on the night of JD 217–218 when turbulent mixing was stronger than usual. The three brief, positive and counter-gradient fluxes of O_3 (on JD 215, 216 and 217) occur at sundown during periods of atmospheric stability transition. These occurrences are associated with increase in relative humidity and vertical O_3 concentration gradient, decrease in air temperature, wind speed and O_3 concentration and (except on day 216) coincide with brief positive perturbations in both R_n and $\int_0^h \frac{\partial \bar{c}}{\partial t} \delta z$. Similar but weaker flux changes also occur on JD 213 and 214 at the same time of day. Summertime counter-gradient O_3 fluxes have previously been reported at this site (Zeller and Hehn, 1994, 1996).

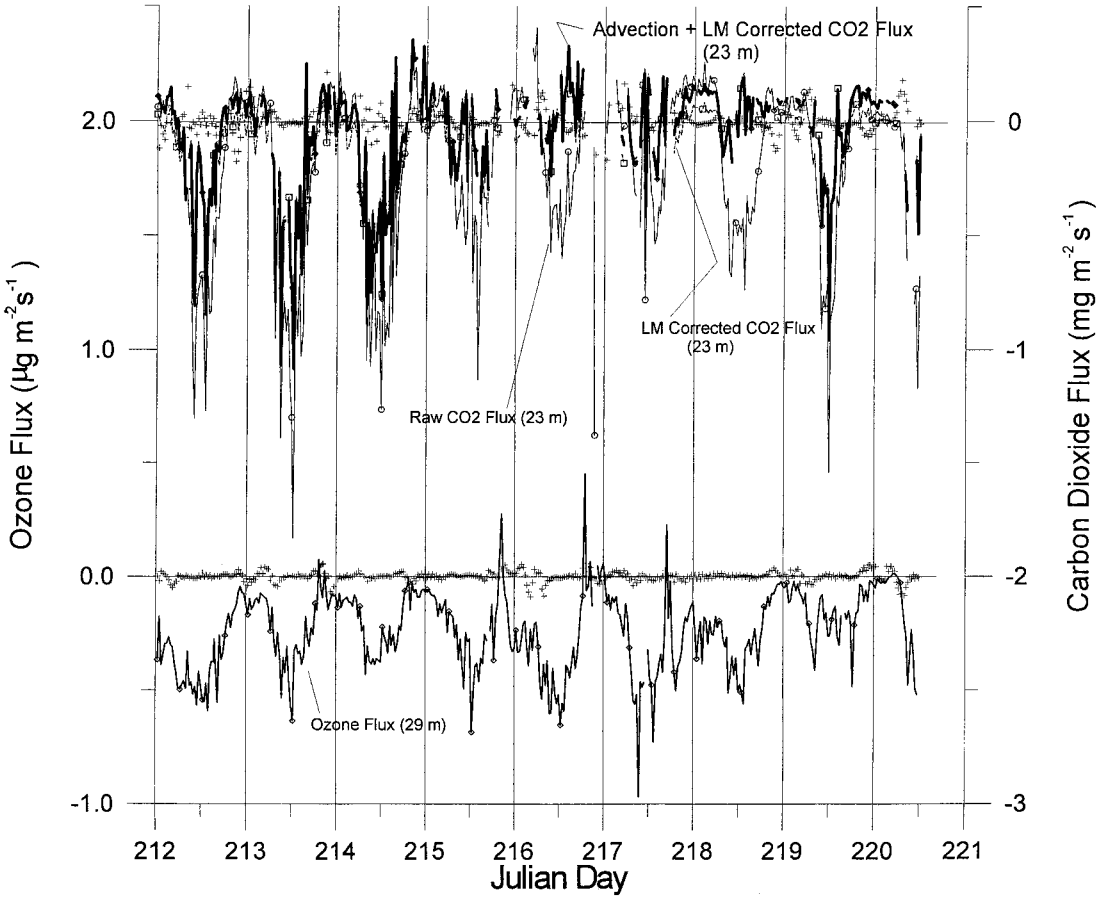

Fig. 8. Half-hour average 23 m CO_2 flux: (1) as measured (raw) (thin solid line, open circle), (2) with sensible and latent heat LM (Leuning and Moncrieff, 1990) corrections (dashed line, open square), and (3) with LM correction and advection correction (heavy solid line, open diamond); 29 m O_3 flux (solid line, open diamond); and local time-rate-of-change value for CO_2 and O_3 (plus signs) for the period 30 July –8 August, 1996.

3.6. Comparison of measured fluxes with model simulations

The FORFLUX model was run for the nine measurement days using observed standard weather data at GLEES, published site characteristics from Musselman (1994) (Table A2) and derived species physiological parameters (Table A1). Due to the lack of information, values of physiological parameter for Engelman spruce were estimated from corresponding data for Douglas fir (Nikolov, 1997).

Figs. 9 and 10 illustrate the comparison of modeled and measured fluxes of CO_2, O_3 and latent heat. The model closely mimics daytime CO_2 flux on days 212–214. However, it predicts higher values at night. On the night of JD 219–220, it closely mimics the CO_2 flux while somewhat approximating the JD 219 daytime flux. It also does a good job for the night of JD 217–218 when a strong turbulent mixing prevailed. However, on days 215–218 and 220, measured and modeled daytime CO_2 fluxes are quite different. Although we do not assume that the model is perfectly accurate, it is likely that the eddy covariance system is just not properly registering the actual CO_2 flux during these times. This conclusion is supported by the fact that a substantial downward flux of O_3 is both modeled and measured on days 215–218. The magnitude of this O_3 flux suggests a high canopy stomatal conductance and, hence, a high CO_2 uptake during these days. In other words, the measured corrected CO_2 flux does not seem to be consistent with the observed O_3 deposition on days 215–218. The correlation between modeled and measured hourly CO_2 fluxes for the entire sampling period is $r^2 = 0.29$ with a slope of 0.7 ± 0.06; intercept of -0.1 ± 0.25; and root mean square error (RMSE) of 0.27. The same statistics for days 212–214 is $r^2 = 0.58$, slope 0.8 ± 0.06, intercept 0.01 ± 0.2 and RMSE 0.219. Since the CO_2 measurements were made 6 m the above canopy, i.e. well within the turbulent mixing layer, these results corroborate the observations of Lee (1998) and Baldocchi (personal communication) for the need to measure CO_2 fluxes close to the canopy top when in rough terrain (Lee et al., 1996). It also appears that it is necessary to sample CO_2 concentrations and wind parameters near the forest floor and at several heights within the canopy to establish scalar profiles and in

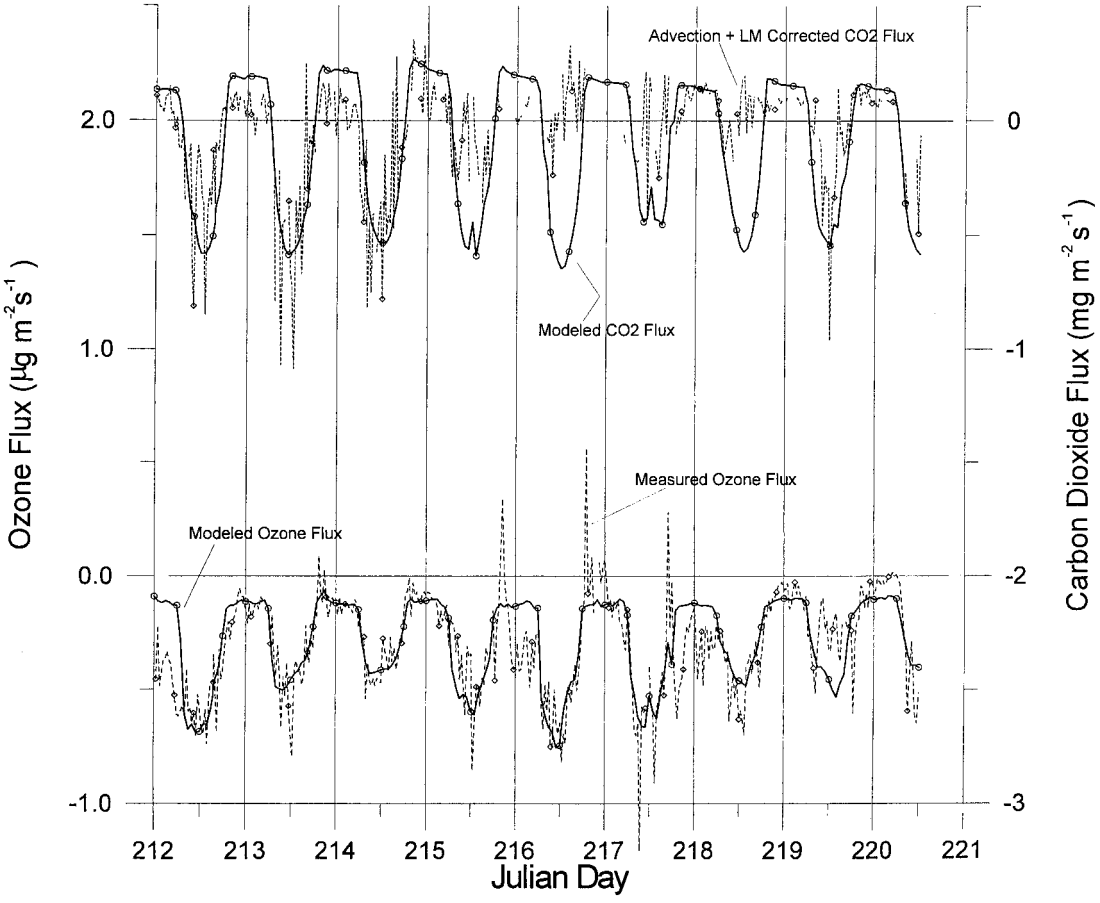

Fig. 9. Half-hour average 23 m CO_2 flux: (1) with LM correction (Leuning and Moncrieff, 1990) and advection correction (dashed line, open diamond) and (2) modeled (solid line, open circle); and 29 m O_3 flux (1) as measured with corrections (dashed line, open diamond), and (2) modeled (solid line, open circle) for the period 30 July–8 August, 1996.

order to adequately correct fluxes for advection and storage effects.

The comparison between modeled and measured O_3 fluxes for the 9-day period is significantly better than that for CO_2 ($r^2 = 0.54$; slope, 0.64 ± 0.03; intercept, -0.09 ± 0.13; RMSE, 0.151). The model successfully tracks observations during most hours. The average measured O_3 flux for the 9-day period is 0.30 μg m^{-2} s^{-1}, which compares rather well with 0.28 μg m^{-2} s^{-1} predicted by the model. Apparently, sampling height is not as much a problem for O_3 as it is for CO_2. Nevertheless, previously reported positive fluxes of O_3 during daytime in the summer by Zeller and Hehn (1996) and the occurrence of occasional positive fluxes in this study, point to the need to correct for possible O_3 advection as well.

Fig. 10 presents the comparison between modeled latent heat flux and measured LE at 12 m above the canopy. Observed daytime maximum values range between 300 and 400 W m^{-2}. These fluxes are somewhat higher compared to 200–300 W m^{-2} measured over a deciduous forest by Greco and Baldocchi (1996) and 150–200 W m^{-2} observed over a boreal black spruce forest by Jarvis et al. (1997). The statistics for the agreement between hourly modeled and measured LE fluxes are: $r^2 = 0.69$; slope, 0.78 ± 0.03; intercept, 21.9 ± 50; RMSE, 53.8. The model predicted an average latent heat flux of 99.6 W m^{-2} for the sampling period. This value is virtually identical with a mean LE of 99.7 Wm^{-2} yielded by the measurements. It appears that sampling height is also not an issue when measuring turbulent water vapor exchange at GLEES.

Based on the above results, we believe that the FOREFLUX model adequately predicted ecosystem–atmosphere exchange of water vapor and O_3 for the nine sampling days at the study site. Due to uncertainties in the CO_2 flux measurements, it is not possible to directly assess the modeled carbon exchange. However, since canopy stomatal conductance is known to exert strong control on all the studied fluxes, and the model

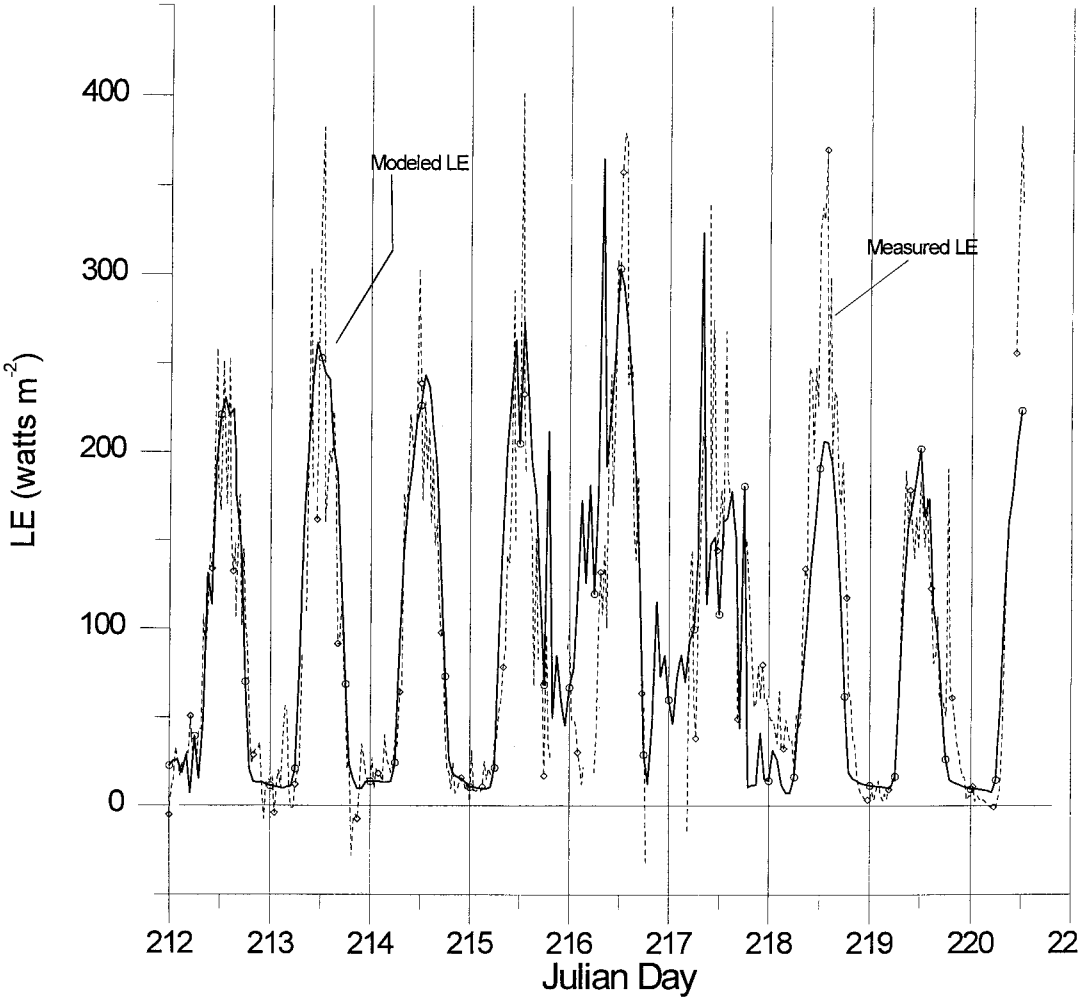

Fig. 10. Half-hour average 29 m latent heat (LE) flux: (1) as measured with corrections (dashed line, open diamond), and (2) modeled (solid line, open circle) for the period 30 July–8 August, 1996.

adequately reproduced evapotranspiration and total O_3 deposition, we assume that it also satisfactorily simulated the CO_2 flux.

3.7. Application of the FORFLUX model to assess annual fluxes at GLEES

The FORFLUX model was used to estimate seasonal dynamics and annual totals of major CO_2, water vapor and O_3 fluxes over this pristine ecosystem. The model was run for a full year using standard hourly meteorological data (i.e. temperature, relative humidity, solar radiation, precipitation) measured at the Brooklyn Tower in 1996, and O_3 concentration recorded for the same time period at a nearby EPA NDDN site. The site-specific and species-physiological parameters required by the model were the same ones used for the verification procedure above (Tables A1 and A2). Based on observations, an initial snowpack depth of 1.6 m was assumed to be present on the site on 1 January 1996. The initial mean soil moisture content was set to 70% of the field capacity value. The latter is estimated in the model from soil texture information.

Fig. 11 depicts simulated seasonal dynamics of the total ecosystem–atmosphere exchange of CO_2, water vapor and O_3 at GLEES for 1996. The model predicts a large fluctuation of daily fluxes for all variables due to variations in meteorological conditions. The daily net ecosystem carbon exchange is estimated to vary from -3.71 to $+0.34$ g C m^{-2} day^{-1} over the growing season having an average value of about -0.53 g C m^{-2} day^{-1} (Fig. 11a). A significant reduction in ecosystem carbon uptake is predicted around day 210 due to an increased CO_2 efflux from soil in response to elevated ground temperature and soil moisture following the snowmelt. Daily evapo-transpiration (ET) ranges from -0.55 to 8.42 mm day^{-1} with negative values caused by vapor condensation on the snow surface (Fig. 11b). ET is noticeable for a smaller seasonal amplitude compared to CO_2 flux. This is a result of a substantial snowpack sublimation during winter and a modest canopy transpiration in the summer.

The total O_3 deposition follows a seasonal pattern, which is distinctly different from that of carbon and water fluxes (Fig. 11c). Daily predicted O_3 uptake by the ecosystem gradually increases from January through to the end of June, and then suddenly leaps by about 100%, staying high throughout the end of August. The

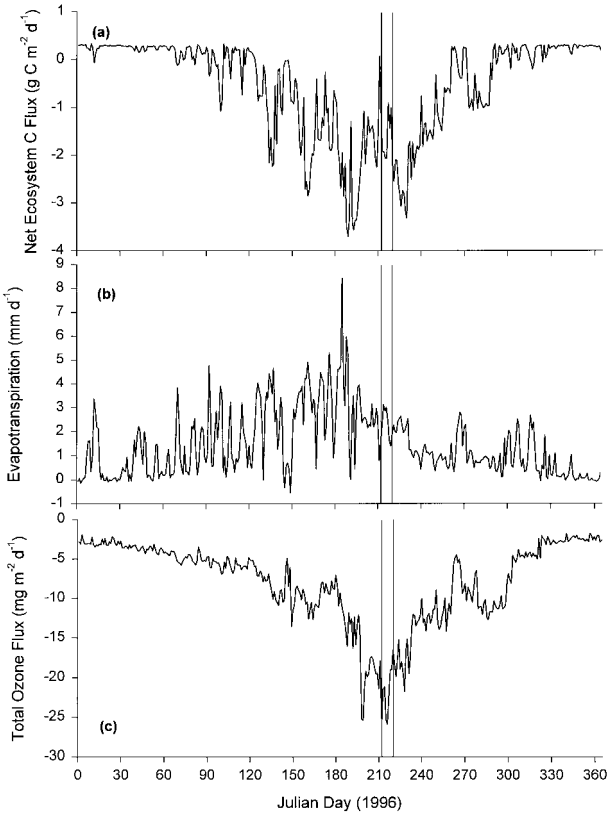

Fig. 11. Seasonal dynamics of daily net ecosystem–atmosphere exchange (NEE) at GLEES predicted by the FORFLUX model in 1996: (a) CO_2 uptake; (b) evapotranspiration; and (c) O_3 deposition.

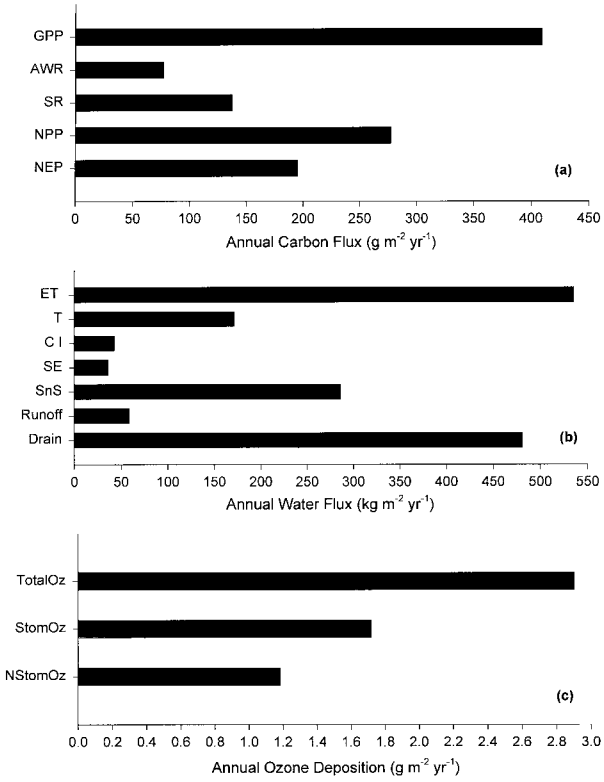

Fig. 12. Component annual fluxes of (a) carbon, (b) water, and (c) ozone predicted by the FORFLUX model at GLEES in 1996 (GPP, net canopy photosynthesis; AWR, Above-ground woody respiration; SR, soil respiration; NPP, net primary production; NEP, net ecosystem production; ET, evapo-transpiration; T, transpiration; CI, canopy rainfall interception; SE, soil evaporation; SnS, snow sublimation; runoff, surface runoff; drain, subsurface drainage; TotalOz, total ozone deposition; StomOz, ozone uptake by leaf stomata; NStomOz, ozone deposition to non-transpiring plant surfaces.

rate of predicted O_3 deposition is relatively low in winter and spring due to the presence of a snowpack on the ground. Snow possesses about a 10-time higher resistance to O_3 exchange than soils. Snowpack also prevents soil from warming up in early spring, which has a negative impact on plant stomatal conductance in the model reducing the O_3 uptake by vegetation. The daily O_3 deposition rate at GLEES varies from 1.8 to 25.9 mg m^{-2} day^{-1} over the course of the year. The magnitude of O_3 fluxes predicted in summertime is consistent with measurements made by Zeller and Hehn (1996) in July of 1992. The subalpine ecosystem was predicted to destroy O_3 at an average rate of 7.92 mg m^{-2} day^{-1} in 1996.

Fig. 12 presents component annual fluxes of the three scalars predicted by the FORFLUX model at GLEES in 1996. Net ecosystem–atmosphere exchange of carbon (NEP) is 195 g m^{-2} $year^{-1}$ while net primary production of vegetation (NPP) is 277 g m^{-2} $year^{-1}$. NEP is less than NPP because it includes the heterotrophic soil respiration. These rather low productivity values are in agreement with the observed slow growth rate of trees in the Medicine Bow Mountains (Earle, 1993). Predicted NPP is also consistent with values reported for boreal forest stands (e.g. Moore, 1996; Ryan et al., 1997). The low NPP and retarded tree growth are attributed to the harsh alpine environment characterized by a cool and short growing season. NEP and NPP are estimated to be 47.8 and 67.7% of the net canopy photosynthesis (or GPP), respectively.

The modeled cumulative ET is 535 mm $year^{-1}$ (Fig. 12b), which represents about 68% of the annual precipitation. Transpiration (174 mm $year^{-1}$) is only 32% of ET, and amounts to about 60% of the annual sublimation from snow. Surface runoff totals 59 mm $year^{-1}$, most of which occurs during a short period in early summer after a rapid snow melt. The model suggests that most of the water released to the atmosphere by this subalpine ecosystem in 1996 came from snow and soil (i.e. ground evaporation represents ca. 60% of ET). Due to a relatively shallow soil column, the runoff is heavily dominated by subsoil drainage.

The model predicted a total O_3 deposition of 2.9 g m^{-2} $year^{-1}$ to GLEES in 1996. About 59% of this amount, or 1.72 g O_3 m^{-2} $year^{-1}$ is projected to be actively taken up by the foliage via leaf stomata. This is the O_3 that comes into direct contact with leaf mesophyle cells and can adversely affect plant photosynthesis and growth. A flux of 1.18 g O_3 m^{-2} $year^{-1}$ is estimated to be deposited to non-transpiring surfaces such as tree stems, branches, snow and soil.

The relatively large portion of non-stomatal O_3 uptake (i.e. about 41% of the total flux) suggests that, when assessing pollution-induced vegetation damage, one needs to relate plant response to the *actively assimilated O_3* by foliage rather than to total deposition. In this regard, we propose a practical index for quantifying vegetation vulnerability to O_3 injury called Physiological O_3 Uptake Per Unit of Leaf Area (POUPULA). It is a ratio of the time-integrated canopy O_3 uptake by plant stomata to the one-sided LAI of the stand. Musselman and Massman (1999) proposed a similar flux-based index to assess O_3 effects on vegetation. The operational implementation of their index, however, is currently impaired by the lack of quantitative information about plant defense mechanisms. POUPULA is not directly measurable on the field but it can be quantified using process models or derived from observed total O_3 deposition amounts. Thus, we estimate POUPULA to be 0.614 g O_3 m^{-2} leaf area $year^{-1}$ for GLEES in 1996. Since this index depends on both species physiology and the physical environment, its value is expected to vary among sites and between years on a particular site. It is, therefore, a future research goal to determine the spatial and temporal variability of this index and to interpret its values in terms of critical thresholds of O_3 uptake for important vegetation types.

4. Conclusion

Measuring carbon exchange has proven to be problematic at GLEES. This is partly because the eddy covariance technique employed above the canopy tends to undermeasure the nighttime ecosystem respiration. Three possible mechanisms have been proposed to explain the poor detection of respiratory CO_2 flux above the canopy: (1) cool, heavier air containing CO_2 may sink to the forest floor at night and advect/meander away under stable atmospheric conditions (Baldocchi et al., 1996; Lee et al., 1996); (2) vertical waves of air associated with stable wind shear can cause advection of pockets of CO_2 (Lee et al., 1996); and (3) the possible inability of the data correction algorithms to accurately account for the 3-dimensional CO_2 flow in mountainous terrain.

The corrected CO_2 flux measured at the GLEES Brooklyn tower shows a reasonable late-summer behavior on certain days and some nights but rarely for a complete 24-h period. The maximum daytime CO_2 fluxes over this subalpine spruce–fir forest ecosystem are -0.7 ± 0.1 mg m^{-2} s^{-1} while night-time exchange varied between 0.2 and 0.3 ± 0.2 mg m^{-2} s^{-1}. This experiment has demonstrated the necessity to address CO_2 advection and storage in future measurements at this site. An empirical correction adapted from Lee (1998) (Baldocchi, personal communication) is employed here in an attempt to address the night-time flux measurement problem. We have found that biophysical models might be useful when assessing eddy flux measurements made in rough terrain. Future CO_2 flux measurements at GLEES should be made closer to the canopy top. Such measurements will also require a detailed study of the diel CO_2 profile changes below the sampling height to

determine how many additional CO_2 concentration measurements must be made to accompany the flux corrections for advection and storage and to provide a valid data set for model validation. Our experience at GLEES suggests that the goal of accurately measuring net CO_2 flux should be either limited to very carefully chosen sites, or require an extensive set of simultaneously collected auxiliary CO_2 and meteorological data.

Both model simulations and measurements suggest that, in early August of 1996, the maximum daytime O_3 deposition rates were -0.5 to -0.6 μg m^{-2} s^{-1}. These results compare well with peak fluxes of -0.3 to -0.6 μg m^{-2} s^{-1} reported for GLEES in July 1992 by Zeller and Hehn (1996). The choice of above canopy measurement height does not appear to be critical for O_3 fluxes. However, previous O_3 flux measurements indicate that advection should also be studied, particularly if the occasionally measured counter-gradient fluxes are to be understood.

The measured sensible and latent heat fluxes are reasonable and agree well with model predictions. They provide some measure of confidence given the obtained energy balance closure. Future experiments at this site should account for heat storage within the canopy.

The FORFLUX model predicted the following annual fluxes for GLEES in 1996: 195 g m^{-2} $year^{-1}$ NEP; 277 g m^{-2} $year^{-1}$ NPP; 535 mm $year^{-1}$ ET; and 2.9 g m^{-2} $year^{-1}$ total O_3 deposition (with an estimated uptake by leaf stomata of 1.72 g O_3 m^{-2} $year^{-1}$). The potential ability of the model to discriminate between total O_3 deposition and physiological O_3 uptake by foliage could provide a valuable tool for researchers who seek to relate pollution-induced vegetation damage to specific uptake amounts rather than to ambient O_3 concentration. In this regard, we introduce for more testing POUPULA, as a practical index for assessing vegetation vulnerability to O_3 injury. This indicator quantifies the amount of O_3 that comes into direct contact with plant photosynthetic machinery and, thus, is mostly responsible for the observed decline in vegetation productivity and crop yield.

Acknowledgements

This study was supported in part by an appointment to the Oak Ridge National Laboratory Postdoctoral Research Associates Program administered jointly by the Oak Ridge National Laboratory and the Oak Ridge Institute of Science and Education. The authors acknowledge the vision of Dr. Douglas Fox (retired from USDA FS), who established GLEES, initiated eddy flux measurements at GLEES and encouraged the development of the FORFLUX model. The authors are also particularly indebted to Ted Hehn from the Department of Renewable Resources, University of Wyoming (formerly with the USDA FS/Rocky Mountain Research Station) for providing the technical electronic and air chemistry support during experiment installation, data collection and instrument maintenance and calibration.

Appendix A
FORFLUX model input parameters and values used

Table A1
Input species physiological parameters used in the FORFLUX model for Engelman spruce (*Picea engelmannii*)[a]

Parameter	Symbol	Units	Value
Maximum carboxylation velocity at 25°C	V_{m25}	mol m^{-2} s^{-1}	59.0
Light-saturated potential rate of electron transport	J_{m25}	mol m^{-2} s^{-1}	108.0 at 25°C
Activation energy for electron transport	E_j	J mol^{-1}	37,000
Kinetic parameter for CO_2 at 25°C	K_{c25}	mol mol^{-1}	22×10^{-5}
Kinetic parameter for O_2 at 25°C	K_{o25}	mol mol^{-1}	0.41
Photosynthetic light loss factor	f	Decimal fraction	0.50
Composite stomatal sensitivity	m	Dimensionless	14.20
Empirical constant for stomatal conductance	b_{sv}	mol m^{-2} s^{-1}	0.019
Mean needle width	d	m	1.1×10^{-3}
Individual leaf reflectance in the visible wavelength	$\alpha_{f,\ vis}$	Decimal fraction	0.09
Individual leaf transmittance in the visible wavelength	$\tau_{f,\ vis}$	Decimal fraction	0.04
Individual leaf reflectance in the near infrared wavelength	$\alpha_{f,\ nir}$	Decimal fraction	0.50
Individual leaf transmittance in the near infrared wavelength	$\tau_{f,\ nir}$	Decimal fraction	0.39
Root conductance parameter	a_r	Dimensionless	2.0
Root conductance parameter	b_r	Dimensionless	30.0
Root conductance parameter	c_r	Decimal fraction	0.25
Critical temperature for root conductance	T_{cr}	°C	4.5
Root signal parameter	A_r	μmol kg m^{-6} h^{-1}	12×10^{-6}
Root signal parameter	B_r	m^{-1}	0.026
Root signal parameter	C_r	kg m^{-2} h^{-1}	0.014

[a] For parameter explanation, see Nikolov (1997).

Table A2
Site-specific input parameters of the FORFLUX model for GLEES

Parameter	Symbol	Units	Value
Slope inclination	I_s	Degree	0°
Latitude	L_g	Deg. Min	41°22′N
Altitude	Z_a	m asl	3186
Slope azimuth	A_z	Degree	0°
Ambient CO_2 concentration	C_a	μmol mol^{-1}	363
Ambient O_2 concentration	O_a	mol mol^{-1}	0.29
Mean annual air temperature	$T_{m,o}$	°C	3.0
Mean annual temperature amplitude	—	°C	10.0
Total canopy leaf area index	L_{tot}	m^2 m^{-2}	2.8
Canopy foliage clumping factor	Ω_{cl}	Decimal fraction	0.70
Mean leaf inclination angle	Θ	Degree	57.4
Above-ground sapwood N	N_s	g m^{-2}	3.20
Above-ground C allocation coefficient	δ_a	Decimal fraction	0.50
Fraction of soil CO_2 efflux in root respiration	—	Decimal fraction	0.40
Total soil depth	Z_{max}	m	0.70
Rooting depth	Z_r	m	0.52
Soil bulk density	ρ_{bs}	mg m^{-3}	1.20
Soil sand content	Sa	% of dry weight	47
Soil clay content	Cl	% of dry weight	13
Soil organic C content	C	% of dry weight	0.5
Soil rock content	f_r	% of volume	50
Visible soil reflectance	$\alpha_{s,\ vis}$	Decimal fraction	0.24
Near-infrared soil reflectance	$\alpha_{s,\ vis}$	Decimal fraction	0.30
Soil roughness length	z_o	m	0.01
Water table presence	—	Boolean	False
Initial snow depth	—	m	0.0
Initial surface soil moisture	—	% of field cap.	65
Initial bottom soil moisture	—	% of field cap.	85

References

Aber, J.D., Federer, C.A., 1992. A generalized, lumped-parameter model of photosynthesis, evapotranspiration and net primary production in temperate and boreal forest ecosystems. Oecologia 92, 463–474.

Albini, F.A., 1981. A phenomenological model for wind speed and shear stress profiles in vegetation cover layers. J. App. Meteorol. 20, 1325–1335.

Auble, D.L., Meyers, T.P., 1992. An open path, fast response infrared absorption gas analyzer for H_2O and CO_2. Boundary Layer Meteorology 59, 243–256.

Baldocchi, D.D., Valentini, R., Running, S., Oechel, W., Dahlman, R., 1996. Strategies for measuring and modelling carbon dioxide and water vapour fluxes over terrestrial ecosystems. Global Change Biol. 2, 159–168.

Bonnan, G.B., 1991a. A biophysical surface energy budget analysis of soil temperature in the boreal forests of interior Alaska. Water Resour. Res. 27, 767–781.

Bonnan, G.B., 1991b. Atmosphere–biosphere exchange of carbon dioxide in boreal forests. J. Geophys. Res. 96, 7301–7312.

Businger, J.A., 1986. Evaluation of the accuracy with which dry deposition can be measured with current micrometeorological techniques. J. Clim. and Appl. Meteor. 25, 1100–1124.

Bresler, E., Dagan, G., 1983. Unsaturated flow in spatially variable fields. 2. Application of water flow models to various fields. Water Resour. Res. 19 (2), 421–428.

Camillo, P., 1987. A canopy reflectance model based on an analytical solution to the multiple scattering equation. Remote Sensing of Environ. 23, 453–477.

Campbell, G.S., 1985. Soil Physics with Basics. Transport Models for Soil–Plant Systems. Elsevier Sience, Amsterdam.

Chameides, W.L., Lodge, J.P., 1992. Tropospheric ozone: formation and fate. In: Lefohn, A.S. (Ed.), Surface Level Ozone Exposures and their Effects on Vegetation. Lewis Publications, Chelsea, MI, pp. 5–20.

Dagan, G., 1993. The Bresler–Dagan model of flow and transport: recent theoretical developments. In: Russo, D., Dagan, G. (Eds.), Water Flow and Solute Transport in Soils. Springer-Verlag, Berlin, pp. 12–32.

Dagan, G., Bresler, E., 1983. Unsaturated flow in spatially variable fields. 1. Derivation of models of infiltration and redistribution. Water Resour. Res. 19 (2), 413–420.

Earle, C.J., 1993. Forest Dynamics in a Forest-Tundra Ecotone, Medicine Bow Mountains, Wyoming. PhD thesis, University of Washington.

Feddes, R.A., Kabat, P., Van Bakel, P.J.T., Bronswijk, J.J.B., Halbertsma, J., 1988. Modelling soil water dynamics in the unsaturated zone — state of the art. J. Hydrology 100, 69–111.

Fitzjarrald, D.R., Moore, K.E., 1992. Turbulent transports over tundra. J. Geophys. Res. 97 (D15), 16717–16729.

Grant, R.F., Rochette, P., 1994. Soil microbial respiration at different water potentials and temperatures: theory and mathematical modeling. Soil Sci. Soc. Am. J. 58, 1681–1690.

Greco, S., Baldocchi, D.D., 1996. Seasonal variations of CO_2 and water vapor exchange rates over a temperate deciduous forest. Global Exchange Biology 2, 183–197.

Hillel, D., 1982. Introduction to Soil Physics. Academic Press, Orlando.

Hirose, T., Werger, M.J.A., 1987. Maximizing daily canopy photosynthesis with respect to the leaf nitrogen allocation pattern in the canopy. Oecologia 72, 520–526.

Hirose, T., Werger, M.J.A., Pons, T.L., van Rheenen, J.W.A., 1988. Canopy structure and leaf nitrogen distribution in a stand of *Lysimachia vulgaris* L. as influenced by stand density. Oecologia 77, 145–150.

Jarvis, P.G., Masshededer, J.M., Hale, S.E., Moncrieff, J.B., Rayment, M., Scott, S.L., 1997. Seasonal variaion of carbon dioxide, water vapor, and energy exchange of a boreal black spruce forest. JGR 102 (D24), 28953–28966.

Kerstiens, G., Lendzian, K.J., 1989. Interactions between ozone and plant cuticles. I. Ozone deposition and permeability. New Physiologist 112, 13–19.

Kirschbaum, M.U.F., 1995. The temperature dependence of soil organic matter decomposition, and the effect of global warming on soil organic storage. Soil Biol. Biochem. 27 (6), 753–760.

Lee, X., 1998. On micrometeorological observations of surface–air exchange over tall vegetation. Agric. and Forest Meteorol 91, 39–49.

Lee, X., Black, T.A., den Hartog, G., Neumann, H.H., Nesic, Z., Olejnik, J., 1996. Carbon dioxide exchange and nocturnal processes over a mixed deciduous forest. Agric. and Forest Meteorol 81, 13–29.

Leuning, R., Moncrieff, J., 1990. Eddy-covariance CO_2 flux measurements using open- and closed-path CO_2 analyzers: corrections for analyzer water vapour sensitivity and damping of fluctuations in air sampling tubes. Bdy. Lyr. Met. 53, 63–76.

Male, D.H., Gray, D.M., 1981. Snowcover ablation and runoff. In: Gray, D.M., Male, D.H. (Eds.), Handbook of Snow. Principles, Processes, Management and Use. Pergamon Press, Toronto, pp. 360–436.

Marshall, S.E., 1989. A Physical Parameterization of Snow Albedo for Use in Climate Models. PhD thesis. Department of Geography, University of Colorado.

Massman, W.J., 1983. The derivation and validation of a new model for the interception of rainfall by forests. Agric. Meteorol 28, 261–286.

Massman, W.J., 1987. A comparative study of some mathematical models of the mean wind structure and aerodynamic drag of plant canoipies. Boundary-Layer Meteorol 40, 179–197.

Massman, W.J., 1998. A review of the molecular diffusivities of H_2O, CO_2, CH_4, CO, SO_2, NH_3, N_2O, NO, and NO_2 in air, O_2, and N_2, near STP. Atmos. Environ. 32 (6), 1111–1127.

Massman, W.J., Zeller, K.F., 1988. Rapid method for correcting the noncosine response errors of the Gill propeller anemometer. J. Atm. and Oc. Tech. 5 (6), 862–869.

Massman, W.J., Grantz, D.A., 1995. Estimating canopy conductance to ozone uptake from observations of evapotranspiration at the canopy scale and at the leaf scale. Global Change Biology 1, 183–198.

Massman, W., Fox, D., Zeller, K. Lukens, D. 1990. Verifying Eddy Correlation Measurements of Dry Deposition: A Study of the Energy Balance Components of the Pawnee Grasslands (Gen. Res. Pap. RM-288). USDA Forest Service RMFRES, Ft. Collins, CO.

McMillen, R.T., 1988. An eddy correlation technique with extended applicability to non-simple terrain. Bdy. Lay. Met. 43, 231–245.

McMurtie, R.E., Rook, D.A., Kelliher, F.M., 1990. Modelling the yield of *Pinus radiata* on a site limited by water and nitrogen. For. Ecol. Manage 30, 381–413.

McMurtie, R.E., Leuning, R., Thomson, W.A., Wheeler, A.M., 1992. A model of canopy photosynthesis and water use incorporating a mechanistic formulation of leaf CO_2 exchange. For. Ecol. Manage 52, 261–278.

Moore, T.R., 1996. The carbon budget of boreal forests: reducing the uncertainty. In: Breymemyer, A.I., Hall, D.O., Melillo, J.M., Ågren, G.I. (Eds.), Global Change: Effects on Coniferous Forests and Grasslands. John Wiley, New York, pp. 17–40.

Musselman, R. C. 1994. The Glacier Lakes ecosystem experiments site (GLEES): An Alpine Global Change Research Study Area (Tech. Rep. RM-249). USDA Forest Service RMFRES, Ft. Collins, CO.

Musselman, R.C., Massman, W.J., 1999. Ozone flux to vegetation and its relationship to plant response and ambient air quality standards. Atmos. Environ. 33, 65–73.

Nikolov, N.T. 1997. Mathematical Modeling of Seasonal Biogeophysical Interactions in Forest Ecosystems. PhD thesis, Colorado State University, Fort Collins CO.

Nikolov, N.T., Massman, W.J., Shoettle, A.W., 1995. Coupling biochemical and biophysical processes at the leaf level: an equilibrium photosynthesis model for leaves of C_3 plants. Ecological Modelling 80, 205–235.

Panofsky, H.A., Dutton, J.A., 1984. Atmospheric Turbulence. John Wiley, New York.

Peterjohn, W.T., Mellilo, J.M., Steudler, P.A., Newkirk, K.M., Bowles, F.P., Aber, J.D., 1994. Responses of trace gas fluxes and N availability to experimentally elevated soil temperatures. Ecol. Applications 4 (3), 617–625.

Ray, J.D., Stedman, D.H., Wendel, G.J., 1986. Fast chemiluminescent method for measurement of ambient ozone. Anal. Chem. 58, 598–600.

Ross, J., 1981. The Radiation Regime and Architecture of Plant Stands. Dr. W. Junk Publishers, The Hague.

Running, S.W., Gower, S.T., 1991. FOREST-BGC, A general model of forest ecosystem processes for regional applications. II. Dynamic carbon allocation and nitrogen budgets. Tree Physiol 9, 147–160.

Runnung, S.W., Coughlan, J.C., 1988. A general model of forest ecosystem processes for regional applications. I. Hydrologic balance, canopy gas exchange and primary production processes. Ecol. Modelling 42, 125–154.

Ryan, M.G., Lavigne, M.B., Gower, S.T., 1997. Annual carbon cost of authotrophic respiration in boreal forest ecosystems in relation to species and climate. J. Geophys Res. 102 (D24), 28871–28883.

Schlentner, R.E., Van Cleve, K., 1984. Relationships between CO_2 evolution from soil, substrate temperature, and substrate moisture in four mature forest types in interior Alaska. Can. J. For. Res. 15, 97–106.

Schuttleworth, W.J., 1989. Micrometeorology of temperate and tropical forest. In: Jarvis, P.G., Monteith, J.L., Schuttleworth, W.J., Unsworth, M.H. (Eds.), Forests, Weather and Climate. The Royal Soc., London, pp. 299–334.

Sellers, P.J., 1985. Canopy reflectance, photosynthesis and transpiration. Int. J. Remote Sensing 6 (8), 1335–1372.

Tanner, B.D., Greene, J.P., 1989. Measurement of Sensible Heat and Water Vapor Fluxes Using Eddy Correlation Methods (Final Report, Campbell Scientific Contract No. DAA09-87-D-0038 to US Army Dugway Proving Grounds). Campbell Scientific, Salt Lake City, UT.

Tardieu, F., Davies, W.J., 1993. Integration of hydraulic and chemical signalling in the control of stomatal conductance and water status of droughted plants. Plant, Cell and Environ. 16, 341–349.

Turner, N.C., Waggoner, P.E., Rich, S., 1974. Removal of ozone from the atmosphere by soil and vegetation. Nature 250, 486–489.

van Pul, W.A.J., 1992. The Flux of Ozone to a Maize Crop and the Underlying Soil During a Growing Season. PhD thesis, Department of Meteorology, Agricultural University, Wageningen, Netherlands.

Wigmosta, M.S., Vail, L.W., Lettenmaier, D.P., 1994. A distributed hydrology–vegetation model for complex terrain. Water Resour. Res. 30 (6), 1665–1679.

Wofsy, S.C., Hollinger, D.Y., 1998. Science Plan for Ameriflux: Long-term Flux Measurement Network of the Americas. Nat'l Inst. for Global Envir. Change (NIGEC), [On-line] Available: http://www.esd.ornl.gov/programs/NIGEC/scif.htm.

Wooldridge, G., Zeller, K., Musselman, R., 1997. Ozone concentration characteristics in and over a high-elevation forest site. Theor. Appl. Climatol. 56, 153–164.

Zeller, K., Hehn, T., 1994. Wintertime anomalies in ozone deposition above a subalpine spruce–fir forest. Proceedings of the 4th USDA

Forest Service S. Sta. Chem. Sc.: Research and Applications of Chemical Sciences in Forestry, Feb 1–2, 131–138.

Zeller, K., Hehn, T., 1995. Ozone deposition in a snow-covered subalpine spruce–fir environment. Biogeochemistry of Seasonally Snow-Covered Catchments (Proceedings of a Boulder Symposium, July 1995), IAHS Publ. No. 228, 17–22.

Zeller, K., Hehn, T., 1996. Measurements of upward turbulent ozone fluxes above a subalpine spruce–fir forest. GRL 23 (8), 841–844.

Zeller, K., Massman, W., Stocker, D., Fox, D.G., Stedman, D., Hazlett, D., 1989. Initial results from the Pawnee Eddy Correlation System for Dry Acid Deposition Research (Gen. Res. Pap. RM-282). USDA Forest Service RMFRES, Ft. Collins, CO.